Structure of bacterial 3beta/17beta-hydroxysteroid dehydrogenase at 1.2 A resolution: a model for multiple steroid recognition.

8 AUTHORS, INCLUDING:

Pietro Roversi
University of Oxford
107 PUBLICATIONS   **3,968** CITATIONS

SEE PROFILE

Kurt D. Berndt
Karolinska Institutet
64 PUBLICATIONS   **2,917** CITATIONS

SEE PROFILE

Rudolf Ladenstein
Karolinska Institutet Huddinge
147 PUBLICATIONS   **6,592** CITATIONS

SEE PROFILE

Articles

Structure of Bacterial 3β/17β-Hydroxysteroid Dehydrogenase at 1.2 Å Resolution: A Model for Multiple Steroid Recognition[†,‡]

Jordi Benach,[Δ,§] Charlotta Filling,[||] Udo C. T. Oppermann,[||] Pietro Roversi,[⊥] Gérard Bricogne,[⊥] Kurt D. Berndt,[§,¶] Hans Jörnvall,[||] and Rudolf Ladenstein*,[§]

Karolinska Institutet NOVUM, Center for Structural Biochemistry, S-14157 Huddinge, Sweden, Department of Medical Biochemistry and Biophysics, Karolinska Institutet, SE−171 77 Stockholm, Sweden, Global Phasing Ltd. Sheraton House, Castle Park, Cambridge CB30AX, UK, and Faculty of Natural Sciences, Södertörn University College, SE−141 04 Huddinge, Sweden

ABSTRACT: The enzyme 3β/17β-hydroxysteroid dehydrogenase (3β/17β-HSD) is a steroid-inducible component of the Gram-negative bacterium *Comamonas testosteroni*. It catalyzes the reversible reduction/ dehydrogenation of the oxo/β-hydroxy groups at positions 3 and 17 of steroid compounds, including hormones and isobile acids. Crystallographic analysis at 1.2 Å resolution reveals the enzyme to have nearly identical subunits that form a tetramer with 222 symmetry. This is one of the largest oligomeric structures refined at this resolution. The subunit consists of a monomer with a single-domain structure built around a seven-stranded β-sheet flanked by six α-helices. The active site contains a Ser-Tyr-Lys triad, typical for short-chain dehydrogenases/reductases (SDR). Despite their highly diverse substrate specificities, SDR members show a close to identical folding pattern architectures and a common catalytic mechanism. In contrast to other SDR apostructures determined, the substrate binding loop is well-defined. Analysis of structure−activity relationships of catalytic cleft residues, docking analysis of substrates and inhibitors, and accessible surface analysis explains how 3β/17β-HSD accommodates steroid substrates of different conformations.

Microbial biotransformation of steroid hormones is carried out by dehydrogenases, reductases, hydroxylases, and isomerases (*1, 2*). Some of these activities are constitutive, but several are steroid-inducible (*2, 3*). A bacterial strain, isolated from contaminated soil, shown to degrade polyaromatic hydrocarbons and able to grow on testosterone as the sole source of carbon, was initially classified as *Pseudomonas testosteroni* and later regrouped as *Comamonas testosteroni* (*2, 4*). Biochemical characterization led to the isolation of several inducible enzyme activities from this strain, namely 3α-hydroxysteroid dehydrogenase (EC 1.1.1.50), 3β/17β-hydroxysteroid dehydrogenase (EC 1.1.1.51), and 3-oxo, Δ[4,5]

isomerase (EC 5.3.3.1). Subsequently, pathways leading to the complete degradation of steroids were elucidated (*5−7*) in *P. testosteroni*. The strong correlation between steroid degradation and xenobiotic catabolism was further emphasized by the discovery that *P. testosteroni* was abundant in heavily polluted environments (*8*). These Pseudomonas strains express a variety of xenobiotic metabolizing enzymes (*9, 10*), associated with increased resistance against steroid antibiotics (*11*) mediated by hydroxysteroid dehydrogenases.

Hydroxysteroid dehydrogenases belong to two protein families, aldo-keto reductases (AKR) or short-chain dehydrogenases/reductases (SDR), with the majority of the forms

[Δ] Present address: Department of Biological Sciences, Columbia University, 702 Fairchild Center, MC 2437, 1212 Amsterdam Avenue, New York, NY 10027.

[§] Center for Structural Biochemistry, Karolinska Institutet NOVUM, SE−141 57 Huddinge, Sweden.

[||] Department of Medical Biochemistry and Biophysics, Karolinska Institutet, SE−171 77 Stockholm, Sweden.

[⊥] Global Phasing Ltd. Sheraton House, Castle Park, Cambridge CB30AX, UK.

[¶] Faculty of Natural Sciences, Södertörn University College, SE−141 04 Huddinge, Sweden.

[1] Abbreviations: HSD, hydroxysteroid dehydrogenase; SDR, short-chain dehydrogenases/reductases; AKR, aldo-keto reductases; 17β-HSD1, human 17β-hydroxysteroid dehydrogenase type 1; NAD⁺, nicotinamide adenosine dinucleotide; PCR; polymerase chain reaction; SDS/PAGE, sodium dodecyl (lauryl) sulfate−polyacrylamide gel electrophoresis; PEG, poly(ethylene glycol); DTT, dithiothreitol; Ac, acetate; MES, 2-(*N*-morpholino)ethanesulfonic acid; TRIS, tris(hydroxymethyl)aminomethane; MPD, 2-methyl-2,4-pentanediol; NCS, noncrystallographic symmetry; daidzein, 7-hydroxy-3-(4-hydroxyphenyl)-4*H*-1-benzopyran-4-one, 4′,7-dihydroxyisoflavone; PDB, protein data bank (http://www.rcsb.org/pdb/); k_{cat}, catalytic constant; K_M, Michaelis constant; −OH, hydroxyl; oxo, carbonyl; C₄N, nicotinamide carbon 4 in NAD(H); F, structure factor amplitude; F_o, observed structure factor; F_c, calculated structure factor; rmsd, root-mean square deviation; carbenoxolone, 3β-hydroxy-11-oxo-20β-olean-12-en-29-oic acid hydrogen butanedioate; TES/testosterone, (17β)-17-hydroxyandrost-4-en-3-one; IU5/isoUDCA, 3β,12α-dihydroxy-5β-cholanoic acid

Table 1: X-ray Collection Statistics

	data set $P3_21$	data set $P2_12_12_1$ at 2 Å	data set $P2_12_12_1$ at 1.2 Å
a, Å; b, Å; c, Å	122.8, 122.8, 78.2	80.1, 110.5, 115.7	80.0, 110.6, 115.1
angles	$\alpha = \beta = 90°, \gamma = 120°$	$\alpha = \beta = \gamma = 90°$	$\alpha = \beta = \gamma = 90°$
space group	$P3_221$	$P2_12_12_1$	$P2_12_12_1$
molecules/au	dimer	tetramer	tetramer
total reflections	83 879	573 102	1 409 412
unique reflections	12 798	70 744	314 581
completeness, % (range, Å)	92.2 (106.3−3.0)	99.5 (85.0−2.0)	94.3 (40.0−1.18)
last shell[a]	88 (3.1−3.0)	94.5 (2.04−1.98)	83.9 (1.25−1.22)
R-merge,[b] % (range, Å)	7.4 (106.3−3.0)	4.0 (85−2.0)	6.9 (40.0−1.18)
last shell	23.0 (3.1−3.0)	22.3 (2.04−1.98)	38.3 (1.25−1.22)
$I/\sigma > 2$, % (range, Å)	87.0 (106.3−3.0)	89.1 (85−1.98)	79.5 (40.0−1.18)
last shell	88.1 (3.1−3.0)	83.3 (2.04−1.98)	54.6 (1.25−1.22)
redundancy	3.6	7.0	4.0
source	711[c]	XW7A[d]	XW7B[d]
wavelength, Å	0.9960	1.0289	0.8424

[a] Only data to 1.22 Å were used. [b] R-merge $= \sum_i I_i - \langle I_i \rangle / \sum_i \langle I_i \rangle$, where I_i is the scaled intensity of the ith observation and $\langle I_i \rangle$ is its mean intensity. [c] Max-lab, Lund, Sweden. [d] EMBL Outstation Hamburg, Germany.

grouped into the latter (*12, 13*). Both families contain prokaryotic and eukaryotic members, and both share a similar reaction mechanism, despite different folding patterns and active-site architectures (*13, 14*). The *C. testosteroni* hydroxysteroid dehydrogenases are SDR enzymes (*15−17*), with similar nucleotide binding sites and active site residues. The 3β/17β-hydroxysteroid dehydrogenase (3β/17β-HSD) is a tetrameric NAD(H)-dependent enzyme, displays 3β- and 17β-OH dehydrogenase and corresponding oxo-reductase activities with androgens, estrogens and *iso*bile acids, and also mediates morphine dehydrogenase activity (*18−20*). Kinetic investigations have revealed an ordered mechanism (*21*) and suggested a single catalytic site accommodating both the 3β- and 17β- activities (*22*). We have reported the crystallization of this enzyme (*23*) and now present the 1.2 Å resolution structure of the apoenzyme, analyze structure−function relationships, and establish the influence of point mutations.

EXPERIMENTAL PROCEDURES

Purification and Mutagenesis of Recombinant 3β/17β-HSD. Molecular cloning of 3β/17β-HSD (EC 1.1.1.51) from *C. testosteroni* ATCC 11996 (Deutsche Sammlung für Mikroorganismen, Braunschweig, Germany) was carried out by generation of a PCR product from genomic DNA, which introduced an N-terminal His-tag with an integrated thrombin cleavage site (*23*). Purification was carried out by a combination of affinity chromatography, thrombin cleavage, and ion exchange chromatography (*23, 24*). Purity was confirmed by SDS/PAGE, and protein concentrations were determined spectrophotometrically using an extinction coefficient of 18 020 M^{-1} cm^{-1} for the monomer. Site-directed mutagenesis was carried out using either the "phosphorothioate" or a PCR-based method (*24*). Mutant sequences were confirmed by cycle sequencing (Big Dye, Applied Biosystems) and analyzed using an ABI 377 system.

Enzymatic Activities of 3β/17β-HSD and Mutant Forms.

Activities were measured as NAD(H)-dependent 3β-and 17β-oxidoreductase activities by the absorbance at 340 nm,

using a molar extinction coefficient of 6.22 mM^{-1} cm^{-1} for NADH (*24*). Steroids for activity measurements were testosterone (17β-HSD), androsterone (17-oxoreductase), 3β,-12α-dihydroxy-5β-cholanoic acid (isoursodeoxycholic acid, isoUDCA, 3β-HSD), dehydroepiandrosterone (3β-hydroxy-5-androsten-17-one, 3β-HSD), and 5α-dihydrotestosterone (3-oxoreductase). Determinations of K_M and k_{cat} values for the substrates and coenzyme were determined as described (*24*). Binding of NADH was assessed by monitoring fluorescence energy transfer as a function of cofactor concentration (*25*) in 20 mM Tris-HCl, pH 7.0 at 298 K using a Shimadzu RF-5000 spectrofluorometer. Binding of NAD$^+$ was determined in a similar manner by displacement of enzyme-bound NADH. Dissociation constants were obtained by nonlinear regression using a 1:1 binding model.

Crystallization and Data Collection. Two crystal forms (trigonal and orthorhombic) of *C. testosteroni* 3β/17β-HSD were obtained from different crystallization conditions. Experiments were performed at 277 K by employing the vapor diffusion technique. Crystals of the trigonal form were obtained from 100 mM NH$_4$Ac, 10 mM DTT, 9% PEG 4000, 50 mM Na-MES at pH 5.5 in the reservoir solution. Orthorhombic crystals were grown at a protein concentration of 7.9 mg/mL, buffered by 50 mM Tris-HCl, pH 7.5, and containing 10 mM DTT. Crystals appeared after several days using 10% ethanol, 250 mM NaCl as reservoir solution and usually grew for several weeks. They were mounted in a fiber loop and flash-cooled in a 100 K nitrogen stream in the presence of 15% MPD (orthorhombic) or 15% glycerol (trigonal) as cryoprotectant. The simulated precession pictures of the raw data in space group *P*1, plotted with the program PATTERN (*26*), pointed to space groups $P3_121$ or $P3_221$ for the trigonal data set and to $P2_12_12_1$ for the orthorhombic set. All data sets are summarized in Table 1. We tried to obtain crystals as binary and ternary complexes with NAD(H), steroids, or inhibitors, but soaking destroyed the crystals even at low coenzyme/substrate concentrations, and cocrystallization yielded poorly diffracting crystals.

Crystal Structure Determination and Refinement. In preliminary crystallographic studies on 3β/17β-HSD (*23*), the refined crystal structure of 3α/20β-hydroxysteroid dehydrogenase from *Streptomyces hydrogenans* (*27*) (PDB accession code 2hsd) was chosen as the search model for molecular

or isoursodeoxycholic acid; AND, 3β-hydroxy-5-androsten-17-one; ANA, 3α-hydroxy-5-androsten-17-one; DAI/daidzein, 7-hydroxy-3-(4-hydroxyphenyl)-4*H*-1-benzopyran-4-one 4′,7 dihydroxyisoflavone; PYR, 5α-androstan-17α-methyl-17β-ol-3,4-pyrazole.
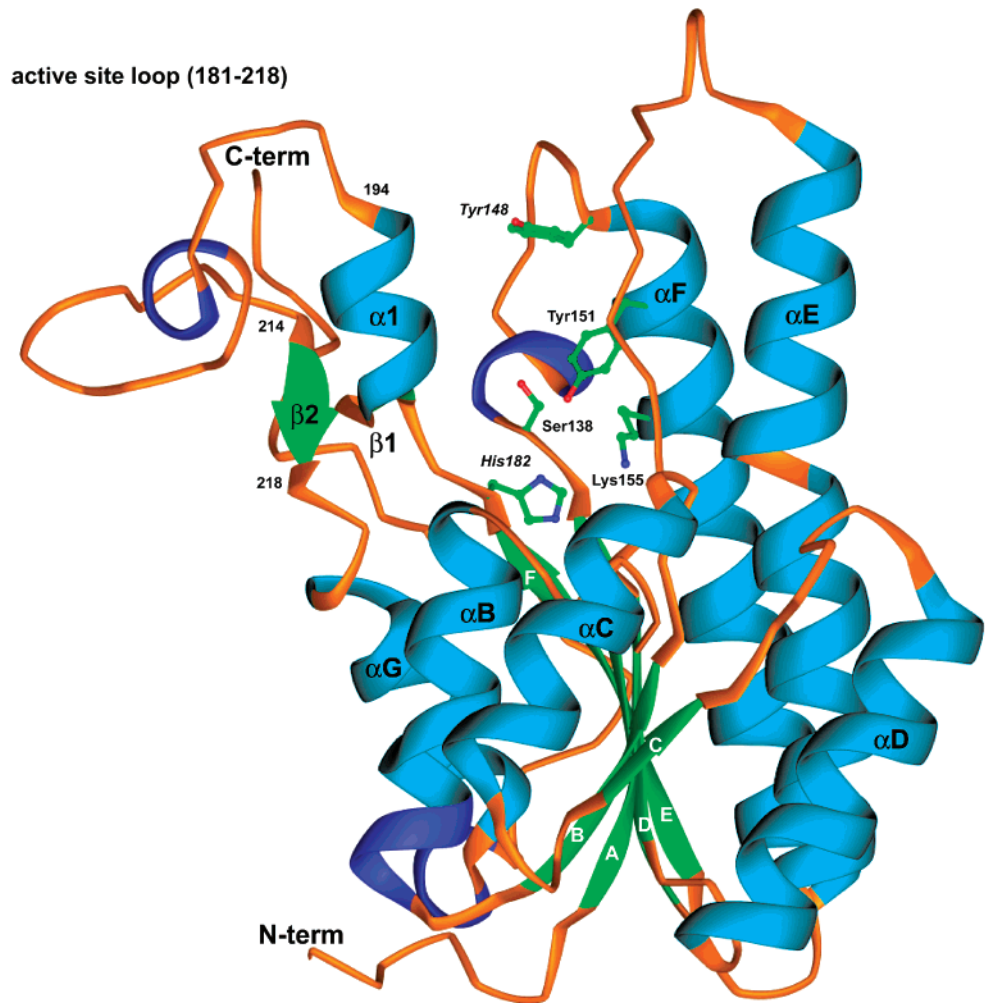
FIGURE 1: Structural organization of 3β/17β-HSD. Ribbon representation of the 3β/17β-HSD monomer. The two residues mutated in this work, Tyr148 and His182, are shown in relation to the active site residues (Ser138, Tyr151, and Lys155). All figures and accessible surfaces herein were produced with the help of RIBBONS (*52*) and VOIDOO (*53*).

replacement. Cross-rotation and translation searches in AMORE using that model (*23*), and the trigonal data set clearly indicated $P3_221$ as the correct space group. The molecular model was improved by manual model building and crystallographic refinement, using REFMAC (*28*). The model refined in REFMAC was taken as the starting structure for a first round of positional and *B*-factor refinement with the program BUSTER-TNT (*29*−*31*), using hard NCS constraints; the NCS operators were computed for the N-terminus (residues 3−184) and C-terminus (residues 216−253) separately from the model refined in REFMAC. A bulk solvent correction was computed from a mask around the model with a radius of 2 Å. The scattering from the missing atoms was modeled using an envelope computed from the BUSTER electron density by using the phases from the starting REFMAC model and the bulk-solvent model. A hundred cycles of refinement lowered the free *R*-factor from 40.1% to 34.8%, and the working *R*-factor from 39.4% to 29.2%. After inspection of the electron density and log-likelihood gradient maps, 37 residues were omitted from the refined model, and a maximum entropy calculation was performed starting from a new envelope for the missing atoms, as computed from the refined model and phases. A round of manual rebuilding in the centroid- and maximum entropy maps resulted in a new model for residues 2−138,

Table 2: Summary of Refinement Statistics

resolution range (Å)	20−1.22
non-hydrogen atoms: protein (solvent)	7854 (1222)
R value[a] (*F* > 4σ)(%)	14.6 (13.9)
Free *R*-value (*F* > 4σ) (%)[b]	18.0 (17.2)
rmsd from ideal values	
bond lengths (Å), angles (deg)	0.014, 2.32
dihedral (improper) angles (deg)	23.9 (1.6)
Ramachandran plot (%):	
most favored, allowed (disallowed)	92.4, 7.4 (0.0)
mean *B*-values (Å²)	
Wilson[c]	11.0
all atoms	19.8
subunit: A, B, C, D, solvent	18.9, 16.9, 15.8, 19.4, 32.4
mean coordinate error[d] (Å)	
all atoms	0.060
protein, solvent atoms	0.051, 0.074
main chain, side chain atoms	0.042, 0.061

[a] *R*-value = $\Sigma|F_o - F_c|/\Sigma|F_o|$. [b] 0.6% of reflection data. [c] Calculated from 5 Å to maximum resolution. [d] As obtained by block matrix inversion in SHELXL (*33*).

143−185, and 213−246. A new BUSTER-TNT refinement started at a free *R*-factor of 33.0% and a working *R*-factor of 32.4%, again modeling both the bulk-solvent and the missing atoms using BUSTER-generated envelopes. After 51 cycles, a free *R*-factor of 29.3% and a working *R*-factor of 25.6% was obtained.
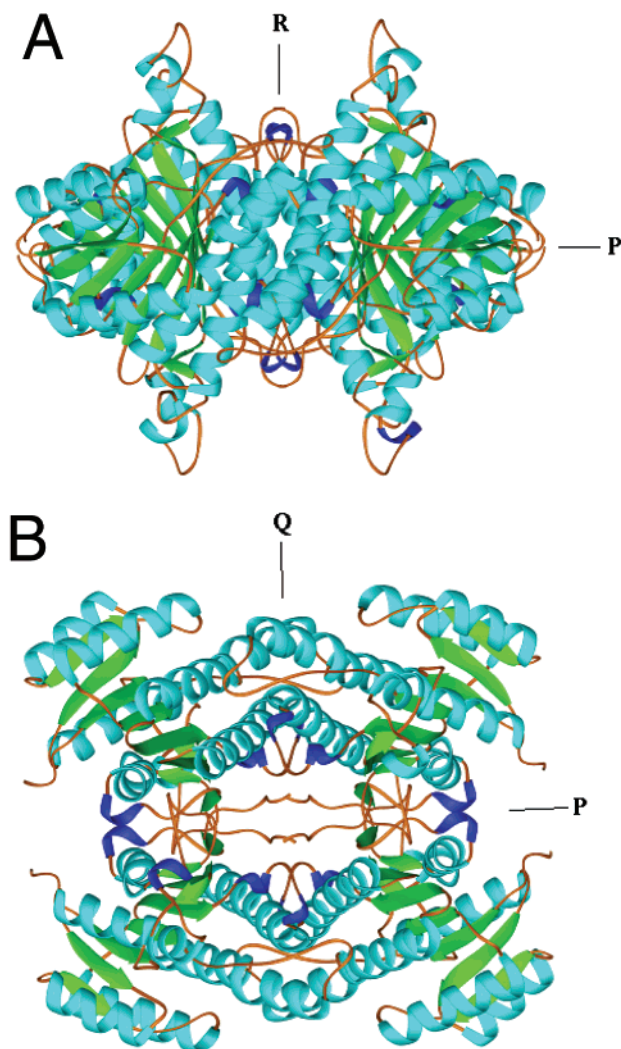
FIGURE 2: The $3\beta/17\beta$-HSD tetramer viewed normal to the Q (A) and R (B) axis.

Table 3: Distances between Atoms at the Active Site of $3\beta/17\beta$-HSD

residue 1	atom 1	atom 2	residue 2	d (Å)	esd[a] (Å)
Tyr151	OH	O	W711	3.15	0.04
Tyr151	OH	O	W472	2.85	0.06
Tyr151	OH	NZ	Lys155	4.30	0.03
Tyr151	OH	OG	Ser138	4.32	0.02
Ser138	OG	O	W409	2.75	0.02
Lys155	NZ	O	W711	3.52	0.04
Lys155	NZ	O	W383	2.88	0.02
Lys155	NZ	O	W155	2.74	0.02
Ile186	N	O	W353	3.01	0.02

[a] As obtained by block matrix inversion in SHELXL (*33*).

The molecular replacement procedure in the space group $P2_12_12_1$ and one tetramer as a search model gave the clearest solution, suggesting that $P2_12_12_1$ is the correct space group. The crystal packing in this space group is very similar to that in the $I222$ data set (*23*). The initial R-value was 45% and was improved by several rounds of model building and crystallographic refinement in CNS and REFMAC to a free R-value of 45% and a working R-value of 41%. Noncrystallographic symmetry averaging was used to improve the electron density maps. Yet, the active site loop region (185−214 in the numbering of $3\beta/17\beta$-HSD), the C-terminal residues, and helices αC and αD were poorly defined. Using the phases from the partially built model, the warpNtrace option in ARP/wARP (*32*) uses the concept of a hybrid model in which protein and free atoms coexist (*32*). Refinement of this hybrid model was carried out in 10 cycles of ARP refinement. The latest map was automatically reinterpreted and the whole procedure was started over for 10−20 cycles at a resolution range of 20−2 Å. The final map was significantly improved, yielding interpretable main-chain and side-chain electron densities of portions of the active site loop (that were completely untraceable before) and other regions such as the C-terminus. After several rounds of model building and manual electron density interpretation, the improved model was subjected to posi-

tional and isotropic B-factor refinement, carried out in REFMAC, and 437 water molecules were included in a cyclic manner by ARP/wARP. At this stage, the working R-value decreased to 29.6% and the free R-value to 32.7%. This refinement was followed by an anisotropic B-factor refinement at the highest resolution of 1.2 Å, and the NCS operators were kept unrestrained. Inclusion of the B-factor anisotropy resulted in a remarkable improvement of the electron density maps, and side chains, which had multiple conformations, were modeled. Finally, several rounds of crystallographic refinement followed by model building were carried out using SHELXL (*33*). Hydrogen atoms were included at this stage as "riding" hydrogen atoms; their positions were calculated stereochemically at the last cycle. To calculate the coordinate error by matrix inversion, conjugate gradient least-squares minimization was carried out using all data sets and splitting the protein structure in five different blocks of 255 amino acids (with three residues overlap). Final statistics of the crystallographic refinement are shown in Table 2.

Substrate/Coenzyme Modeling. The position of the NAD$^+$ and inhibitor molecules of the $3\alpha/20\beta$-HSD binary complexes (*27, 34*) and the accessible surface of $3\beta/17\beta$-HSD were used to build the ternary complexes with NAD$^+$/NADH and substrates (5α-dihydrotestosterone, testosterone, iso-ursodeoxycholic acid, 3β-hydroxy-5-androsten-17-one) or inhibitors (3α-hydroxy-5-androsten-17-one, daidzein, 5α-androstan-17α-methyl-17β-ol-3,4-pyrazole). Three-dimensional structures of the substrates/inhibitors were obtained from the PDB. The model was subjected to 1000−2000 conjugate gradient minimizations cycles in CNS until convergence, where the protein structure was kept unaltered. AUTODOCK (*35*) was used to further refine the substrate or inhibitor position within the active site formed by the protein structure and the coenzyme molecule. Because of slight structural differences between protein subunits, all modeling calculations were performed on all four subunits.

RESULTS

Quality of the Model and Overall Fold. The model of $3\beta/17\beta$-HSD was refined to a working R-value of 14.6% and a free R-value of 18.0% for all data without σ cutoff in the resolution range 20−1.2 Å (Table 2), excluding 0.6% randomly distributed reflections assigned to calculate the free R-value. The asymmetric unit contains a $3\beta/17\beta$-HSD tetramer with each subunit consisting of 253 residues. The model contains 1222 water molecules with B-factors in the range 9−60 Å^2. The most favored regions of the Ramachan-
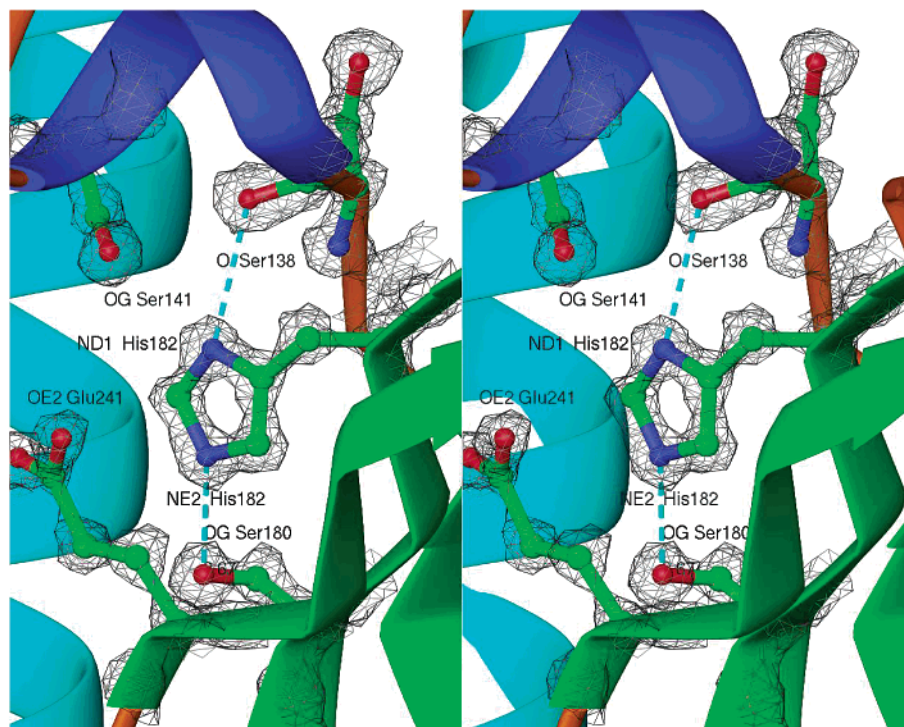
FIGURE 3: Stereoview, showing the mutation site His182Leu. The $2F_o - F_c$ electron density map at 1.2 Å is contoured at 1σ.

dran plot, as defined by PROCHECK (*36*), contain 92.2% of the nonglycine residues.

The polypeptide chain is folded into a single α/β domain (Figure 1). This domain comprises a central parallel β sheet formed by seven β-strands (βC$-$$\beta$A, βD$-$$\beta$G) twisted overall by 45°, with three α helices on either side (αD$-$$\alpha$F and αC$-$$\alpha$G) of the sheet. The βA to βF segment has the typical "Rossmann fold", associated with NAD(H) binding, and in addition, the βD to βG segment is involved in quaternary structure association and substrate binding. The substrate binding loop, a segment consisting of residues 185$-$217 (connecting βF and αG) is well-defined, in contrast to the situation with other SDR apostructures (*27, 37*). The 3β/17β-HSD tetramer shows 222 symmetry (Figure 2) and the tertiary structures of the monomers are nearly identical, with the largest variations found in the loops and terminal regions.

Active Site Architecture. The accessible surface area calculated with a water probe radius of 1.4 Å reveals a deep and extended cleft near the C-terminal ends of the β-strands that constitute the central sheet. In analogy with the three-dimensional structures of other members of the SDR family (*27, 38, 39*), this active site cavity can be clearly separated into the substrate- and the coenzyme-binding sites. The substrate-binding cleft is formed by residues 185$-$217 (active site loop region), together with the C-terminal region of the same subunit, and the C-terminal region of the subunit related through the *R*-axis. The site can be subdivided into an upper and a lower segment. In the upper segment, we find the following residues: Met190, Met191, Ser194, Leu195, Pro196, Val199, Met203, Val204, Asn211, Ala213, Gly214, Arg215 (forming a salt bridge with Asp184), Gly185, and Ile186; Met215 and Gly252 (C-terminal region of the same subunit); and Gly252 and Leu253 (C-terminal of the *R*-axis related subunit). The lower segment of the substrate cleft is formed by the catalytic triad: Ser138, Tyr151, and Lys155

(Table 3). These residues are surrounded by Ser140, Val139, and Asn111.

Three regions can be discriminated within the NAD(H) binding site: (1) the region binding the nicotinamide ring moiety of the coenzyme, surrounded by hydrophobic amino acids (main chains of Ala137 and Met136 and side chains of Pro183 and Ile186) [This apolar environment is concluded to be the reason for the observed fluorescence enhancement by NADH binding to the enzyme (*19*).]; (2) the phosphate groups that interact mainly with a glycine-rich motif (T[12]-GGASGVG[19]) and the main-chain atoms of Ala88 and Gly89, following the SDR sequence fingerprint (*13*); and (3) the adenine moiety interactions with the side chains of Ala88, Ile90, Ile110, Val61, Asp60, Ile38, and Asp37.

Inspection of the apostructure and initial docking experiments revealed several residues of possible importance for catalysis and structural integrity. These residues could be further classified as conserved residues in SDR enzymes (e.g. members of the catalytic triad, Ser138, Tyr151, and Lys155) and some data have been reported earlier (*40, 41*). Other residues were identified to be specific to 3β/17β-HSD with possible implications in substrate binding or catalysis (His182 and Tyr148, cf. below).

His182, located at the end of βF, forms hydrogen bonds to the side chains of Ser141 (distance: 2.9 Å) and Ser180 (2.7 Å) and the main-chain atoms of Ser138 (3.1 Å) and appears to form a salt bridge with the side chain of Glu241 (3.4 Å) (Figure 3). Since the replacement of His182 with Leu results in a significantly altered enzyme (Table 4), these interactions are concluded to be absent in the mutant. The importance of His182 for coenzyme binding is demonstrated by the altered K_d properties of the His182Leu mutant. No saturation of binding up to a concentration of 100 μM NAD$^+$ or NADH is observed, in contrast to the situation with the wild-type enzyme, which has K_d values of 1.5 and 1.0 μM

Table 4: Kinetic Constants for 3β- and 17β-Dehydrogenase Activities of 3β/17β-HSD[a]

	3β-HSD									17β-HSD					
	isoursodeoxycholic acid			dehydroisoandrosterone			3-ketoreductase 5α-dihydrotestosterone			testosterone			17-ketoreductase androsterone		
	K_M	k_{cat}	relative k_{cat}/K_M	K_M	k_{cat}	relative k_{cat}/K_M	K_M	k_{cat}	relative k_{cat}/K_M	K_M	k_{cat}	relative k_{cat}/K_M	K_M	k_{cat}	relative k_{cat}/K_M
wild type	22.3[b] ± 3.9	1.4[b] ± 0.1	100[b]	11.4 ± 0.3	0.64 ± 0.2	100	16.1[b] ± 1.2	0.13[b] ± 0.05	100[b]	11.8 ± 2.0	1.2 ± 0.2	100	31.7 ± 2.5	0.21 ± 0.03	100
Tyr148Phe	28.3 ± 2.8	0.73 ± 0.1	41	11.8 ± 0.9	0.65 ± 0.05	98	10.4 ± 1.6	0.13 ± 0.04	150	9.5 ± 1.1	2.5 ± 0.2	260	22.3 ± 1.7	0.28 ± 0.06	190
His182Leu	130 ± 14	0.12 ± 0.03	1.5	15.9 ± 3.4	0.038 ± 0.003	4.3	53.5 ± 5.0	0.027 ± 0.001	6.3	10.8 ± 1.1	0.06 ± 0.02	5.6	27.1 ± 3.1	0.026 ± 0.004	14

[a] Substrates used were isoursodeoxycholic acid or dehydroisoandrosterone (3β-HSD), 5α-dihydrotestosterone (3-ketoreductase), testosterone (17β-HSD), and androsterone (17-ketoreductase). K_M values are in 10^{-6} M, k_{cat} values are in 10^3 min^{-1}, and relative k_{cat}/K_M values were calculated using wild-type activities as a reference. Values shown are the average of three to five experiments and its corresponding standard deviation. [b] Taken from (24).

Table 5: Apparent Michaelis Constant K_M and K_d for NADH and NAD$^+$ with 3β/17β-HSD Wild-Type and Mutant Proteins[a]

substrate	DHIA	isoUDCA	5α-dihydrotestosterone			
	K_M NAD$^+$	K_M NAD$^+$	K_d NAD$^+$	K_M NADH	K_d NADH	
wild type	28.3 ± 2.1	83.3 ± 3.9	1.5 ± 0.3	21.6[b]±1.9	1.0 ± 0.2	
Tyr148Phe	23.2 ± 3.7	168 ± 6.2	2.6 ± 1.5	12.6 ± 2.1	3.0 ± 1.0	
His182Leu	180 ± 27	484 ± 60	c	25.5 ± 1.3	c	

[a] Values shown (×10^{-6} M) are the average of three to five experiments and its corresponding standard deviation. [b] Taken from (24). [c] No saturation measurable up to the experimental limit of 100 μM.

for NAD$^+$ and NADH, respectively (Table 5). Interestingly, the K_M of NAD$^+$ increases significantly (5−6 times vs WT), whereas the K_M of NADH largely remains unaffected (25.5 vs 21.6) (Table 5). A possible structural explanation for the behavior observed in this mutant is the interactions described above, linking the C-terminal substrate binding region to the active site (Figures 1 and 3). These observations show that residues not directly located at the active site contribute to catalysis in a complex manner through support of correct conformations of the active-site residues.

3β/17β-Stereospecificity and Substrate Recognition. The probe-accessible surface calculated for the apostructure shows a deep cavity that is open to the bulk solvent and close to the catalytic triad (Figure 4A). On one side of the accessible surface, the α-side (left side of Figure 4A), the convex surface easily fits to the concave α-side of a steroid substrate. On the opposite side of the active site cavity, the β-side (right side of Figure 4A), the accessible surface is irregular. Instead, it shows two small subcavities that accommodate the angular methyl groups present on the β-side of the steroid skeleton (at C10 and C13). These features provide the structural basis for the preference of this enzyme toward β-hydroxysteroids rather than α-hydroxysteroids. The overall elongated shape of the cavity is concluded to account for the specificity toward 3β- and 17β-hydroxysteroids. Furthermore, this cleft fits steroids with ring A/B cis fusions (i.e. hydrogen at C5 in the 5β-position as in isoursodeoxycholic acid) or a near planar trans A/B ring structure (hydrogen at C5 in α or double bond between C4 and C5, as in 5α-dihydrotestosterone, testosterone, and androsterone, or between C5 and C6, as in dehydroepiandrosterone). The observed stereospecificity becomes even more apparent when the accessible surface of 3β/17β-HSD is compared with that of another bacterial HSD, the *S. hydrogenans* 3α/20β-HSD. This enzyme presents a more convex α-side that explains why this enzyme does not allow binding of 3β-hydroxysteroids (Figure 4B).

In contrast to other SDR apoforms, we can easily characterize the three-dimensional structure of the active site loop (residues 185−217), allowing us to interpret steroid and inhibitor binding by modeling several ternary complexes [NAD$^+$ and testosterone, androsterone and daidzein, depicted in Figures 4A and 5; others (Table 6) not shown]. The interaction of the substrates and inhibitors with the active site cavity is hydrophobic on the α-side (Met191, Leu195, Val204, Ala216) with the exception of the salt bridge formed by Arg215 and Asp184. On the β-side, we found both hydrophobic and hydrophilic residues: Leu91, Val139, Ser140, Ile145, Gln147, and Tyr148 (Figure 5). The modeled distances of the reactive hydroxyl/carbonyl group at positions
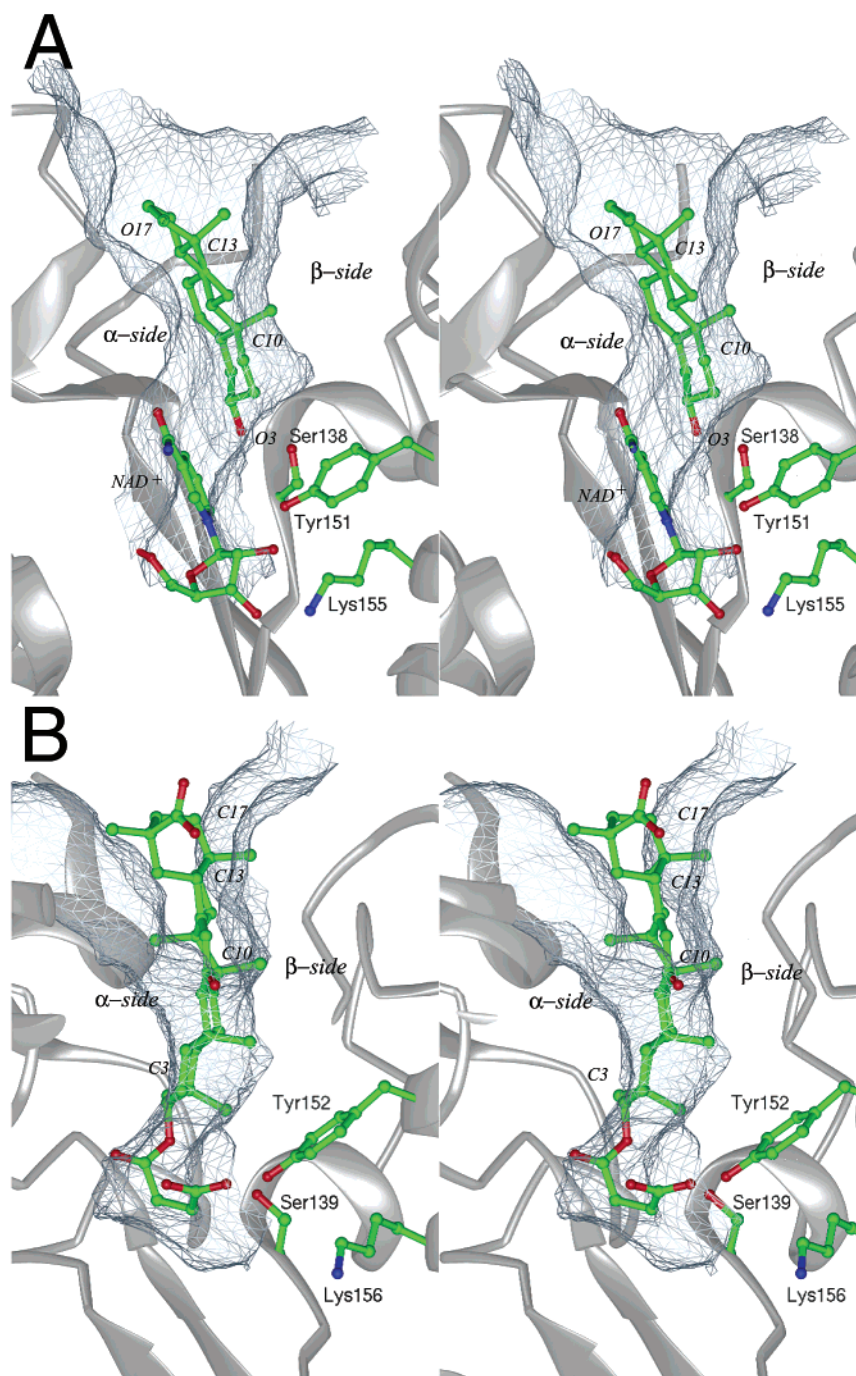
FIGURE 4: Comparison of the probe-accessible surface of the active site of 3β/17β-HSD complexed with NAD+ and 3β-hydroxy-5-androsten-17-one (A) and 3α/20β-HSD (PDB code 1hdc) with carbenoxolone (B).

3 and 17 in the steroid substrates are within the range of a hydrogen-bond interaction to Tyr155 and Ser138 (Table 6). To demonstrate the stereospecificity, we modeled a 3α-OH steroid (3α-hydroxy-5-androsten-17-one) into the active site. In this case, the distances between the nonreactive 3α-hydroxyl group and Tyr155 or Ser138 are larger (6−4 Å) than for the reactive 3β/17β-hydroxyl groups in 3β/17β-OH steroids, thus explaining the catalytic efficiency with the latter but not the former compounds (Figure 5C,D). In the enzyme−inhibitor models with the A ring fused steroid pyrazole [5α-androstan-17α-methyl-17β-ol-3,4-pyrazole (42)] and the isoflavine daidzein (43) (Figure 5E,F), nonreactivity is also explained (Table 6).

Kinetic studies of a Tyr148Phe mutant, located at the surface of the active site cavity (Table 4 and Figures 1 and 5A,C), show the importance of a hydrophobic surface for selective alterations in the catalyzed reactions. Kinetic constants for 3β-OH (substrates, dehydroisoandrosterone and isoursodeoxycholic acid) and 17β-OH (substrate, testosterone) dehydrogenase activities and the reductive activities (3-oxo substrate, 5α-dihydrotestosterone; 17-oxo substrate, androsterone) were measured for the wild-type form and the mutant Tyr148Phe. The Tyr148Phe mutation lowers the 3β-HSD activity (41% residual activity for isoursodeoxycholic acid) or leaves it unchanged (98% for dehydroepiandrosterone compared to wild-type k_{cat}/K_M, Table 4), whereas all other

Table 6: Distances (Å) and Surrounding Residues at the Active Site with Modeled Substrate/Inhibitor Molecules[d]

	reaction	Tyr155[a]	Ser138[a]	hydride[b]	α-side[c]	β-side[c]
DHT	3-ketoreductase	4.03	2.51	3.04	R215, D184, M191, G185	S140, Y148, I145, L91,
TES	17β-HSD	3.07	3.76	2.00	R215, D184, M191, G185, A216, V204	S140, Y148, I145, L91,
IU5	3β-HSD	2.43	2.87	3.46	R215, D184, M191, G185	S140, Y148, I145, L91 Q147
AND	3β-HSD	3.23	3.47	4.30	R215, D184, M191, G185, A216	S140, Y148, I145, L91
ANA	inhibition	5.87	4.11	4.96	R215, D184, M191, G185, A216	S140, Y148, I145, L91
DAI	inhibition	4.01	2.87		R215, D184, M191, G185, A216, V204	S140
PYR	inhibition	5.13	2.62		R215, D184, M191, G185, L195, V204	S140, Y148, V139

[a] Distance from the reactive hydroxyl/carbonyl group to the hydroxyl group of the residue. [b] Distance between the C_4N position in the coenzyme and the transferring hydrogen atom in the substrate. [c] Amino acids within a 4 Å radius from any atom in the substrate/inhibitor; the name for the sides is as defined in the text. [d] DHT, 5α-dihydrotestosterone; TES, testosterone; IU5, isoursodeoxycholic acid; AND, 3β-hydroxy-5-androsten-17-one; ANA, 3α-hydroxy-5-androsten-17-one; DAI, daidzein; PYR, 5α-androstan-17α-methyl-17β-ol-3,4-pyrazole.

activities are enhanced (3-oxo reductase 150%, 17β-OH-HSD 260%, 17-oxo reductase 190%). All K_M values of Tyr148Phe are in the same order as for the corresponding wild-type, pointing to the nonessential nature of Tyr148 for substrate binding. Instead, the observed differential activities are concluded to be a combination of substrate-specific features (substrate position 3 or 17), and altered coenzyme characteristics. The affinity for NADH is increased (12.6 vs 21.6 μM) whereas a substrate-dependent change in K_M for NAD$^+$ is noted for isoursodeoxycholic acid and remains unaltered for dehydroisoandrosterone (Table 5).

Similarities of the Active Site Loop with Other SDRs. When compared to other members of the SDR family, 3β/17β-HSD shares little or no similarity in the active site loop (181−218, in the numbering of 3β/17β-HSD; Figure 1). Any structural homology is concentrated at the beginning (β1,α1, 181−194) or the end (β2, 214−218) of the active site loop. The least conserved region is therefore ranging from residues 194 to 214. This area is often involved in the recognition and orientation of the substrate, and therefore, a high degree of flexibility and structural disparity is required to accommodate the different substrates. The most similar active site loops available in the SDR family are the ones from the other hydroxysteroid dehydrogenases.

Escherichia coli 7α-hydroxysteroid dehydrogenase (44) complexed with NADH and 7-oxo glycochenodeoxycholic acid (PDB code 1fmc) shows a similar active site loop; in this case, however, the C-terminus forms more directly part of the active site cleft by positioning the steroid molecule in the right orientation for the 7α-HSD reaction. Despite the overlapping substrate specificities of human 17β-hydroxysteroid dehydrogenase type 1 (17β-HSD1) (45) to 3β/17β-HSD, the crystal structure of 17β-HSD1 complexed with dihydrotestosterone (PDB code 1dht) displays a very different active site loop when compared to 3β/17β-HSD. In 1dht, the active site loop is formed mostly by two long α-helices that close the active site, showing a dihydrotestosterone molecule in a different orientation in relation to the one modeled in this work. *S. hydrogenans* 3α,20β-hydroxysteroid dehydrogenase complexed with carbenoxolone (PDB code 1hdc) (34) is the most similar to 3β/17β-HSD. The initial α-helix (α1) and the final β-strand (β2) are the most similar secondary motifs between the two enzymes. However, the region from 194 to 214 is different, explaining the specificity toward the different steroids (Figure 4). Finally, one of the most different active site loops is the one belonging to porcine testicular carbonyl reductase/20β-hydroxysteroid dehydrogenase (46), with a well-ordered active site loop.

DISCUSSION

Hydroxysteroid dehydrogenases (HSDs) are essential in the biosynthesis of all classes of mammalian steroids and constitute an important prereceptor signaling pathway (47). This forms the basis for novel concepts in inhibitor development of potential therapeutic value in the treatment of diseases, such as obesity, diabetes, and hormone-dependent cancer, and in fertility control. Since most of these pharmacological targets comprise SDR-type hydroxysteroid dehydrogenases, structural and mechanistic studies of this enzyme family are mandatory to understand structure−activity relationships. In the past, several structural studies resulted in detailed information on reaction and inhibition mechanisms, or substrate specificities (48−50) of SDR enzymes. The structure of bacterial 3β/17β-HSD is one of the largest structures refined at 1.2 Å resolution and provides a tool for the understanding of steroid−protein interactions. Already the apostructure gives information on recognition of different steroid configurations with substituents at position C5. Furthermore, the dual positional specificity of 3β/17β-HSD can be explained by the structure obtained. The remarkable substrate variability of 3β/17β-HSD expands our knowledge on steroid recognition by SDR enzymes, as observed in type 1 17β-HSD (48), 7α-HSD (44), or 3α/20β-HSD (27, 34), which display more strict specificities.

The side-chain conformations of the catalytic triad Tyr151, Lys155, and Ser138 in 3β/17β-HSD are similar to those found in other SDR enzymes (27, 34, 51), suggesting a highly similar catalytic reaction mechanism, in line with kinetic data on 3β/17β-HSD (19, 22). In the dehydrogenation reaction, Tyr151 is likely to be in the deprotonated state because of the electrostatic influence of the positively charged Lys155 side chain and the nicotinamide ring of the oxidized NAD$^+$ molecule. A function of Lys155 is to facilitate the deprotonation of the 3β/17β-hydroxyl group of the steroid molecule and hence to catalyze the hydride transfer step from the 3/17-position of the steroid to the C_4N atom of the coenzyme. In the reduction process, an uncharged NADH nicotinamide ring favors a neutral Tyr151 protonating the steroid molecule. Lys155 and Ser138 would assist in promoting the proper orientation of the coenzyme and substrate molecules, respectively. The essential nature of the latter residue as part of the active site triad in 3β/17β-HSD catalysis has been demonstrated (24). The high-resolution structure has also allowed us to carry out mutagenesis studies on other amino acids close to the catalytic triad, thereby substantially improving our understanding of the enzymatic catalytic mechanism (41).
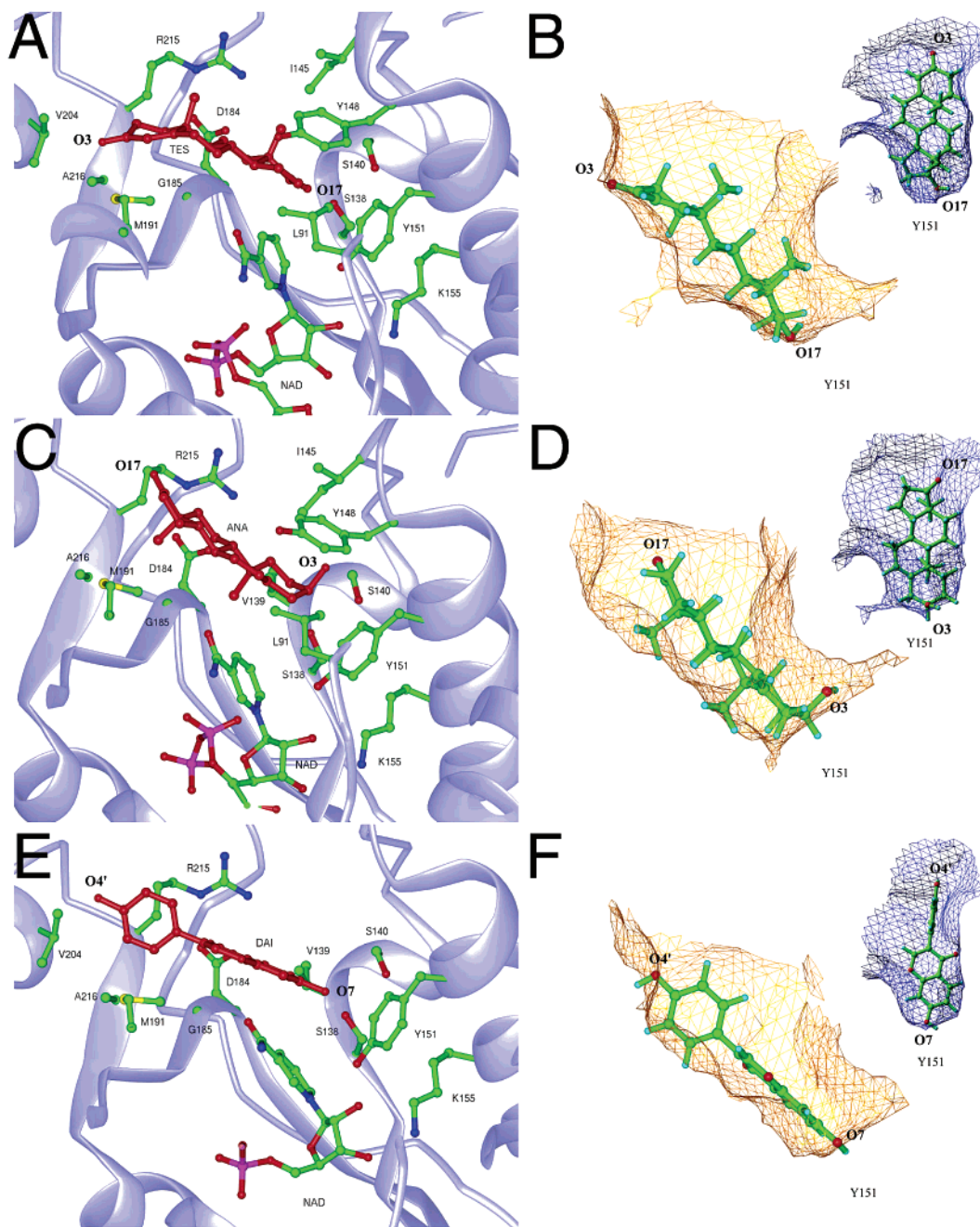
FIGURE 5: Several binding modes for substrates/inhibitors in the active site of 3β/17β-HSD in relation to the catalytic triad and the coenzyme molecule (NAD⁺). The catalytic triad (Ser138, Tyr151, and Lys155) and residues forming van der Waals contact (4 Å) with the substrate/inhibitor are shown (left panels: A, C, D). The complementarity between the different substrate/inhibitor molecules and the accessible surface (probe 1.4 Å) of 3β/17β-HSD (right panels: B, D, F) is shown in two different orientations (in either green or blue); the label Y151 shows where the hydroxyl group of the catalytic site Tyr151 is in relation to the substrate/inhibitor. (A, B) TES (testosterone): 17β-OH dehydrogenase reaction. (C, D) ANA (3α-hydroxy-5-androsten-17-one): 3α-OH dehydrogenase reaction, (E, F) DAI (daidzein): inhibition.

Regarding the nine different molecules fitted at the active site of 3β/17β-HSD, the reactive hydroxyl/carbonyl groups are within or near to hydrogen-bond distances to the catalytically important residues (Ser138 and Tyr151) and in close distance to the hydride atom in the C_4N position of the coenzyme. Furthermore, there is a preference for shorter distances between the steroid and Ser138 (2.51–3.76 Å) than Tyr151 (2.43–4.03 Å, Table 6). This result explains the necessity of a small polar group (Ser or Thr) in that position (24). The latter appears to be crucial for correct binding of steroidal substrates.

The substrate recognition by 3β/17β-HSD is also apparent from the modeled substrates and inhibitors displayed together with the accessible surface of the catalytic site. The hydrophobicity and size of the residues on the α-side of the active site is concluded to be essential in binding the substrates. In contrast, as seen by the effect of the Tyr148Phe mutation, the β-side has a less pronounced effect on substrate binding. We are aware that the crystallographic ternary complexes of 3β/17β-HSD will shed definite light on the steroid binding. However, in the absence of such crystal complexes, careful modeling on a high-resolution structure

and a well-ordered active site pocket has already now proven to be helpful in determining the structural basis for stereospecificity and substrate recognition.

ACKNOWLEDGMENT

REFERENCES

1. Charney, W., and Herzog, H. L. (1967) *Microbial Transformation of Steroids. A Handbook*, Academic Press, New York, London.
2. Talalay, P., Dobson, M. M., and Tapley, D. F. (1952) *Nature 170*, 620−621.
3. Karlson, P. (1983) *Hoppe Seylers Z. Physiol. Chem. 364*, 1067−1087.
4. Tamaoka, J., Duk, H., and Komagata, K. (1987) *Int. J. Syst. Bacteriol 37*, 52−59.
5. Shaw, D. A., Borkenhagen, L. F., and Talalay, P. (1965) *Proc. Natl. Acad. Sci. U S A. 54*, 837−844.
6. Coulter, A. W., and Talalay, P. (1968) *J. Biol. Chem. 243*, 3238−3247.
7. Coulter, A. W., and Talalay, P. (1967) *Biochem. Biophys. Res. Commun. 29*, 413−417.
8. Garcia-Valdes, E., Cozar, E., Rotger, R., Lalucat, J., and Ursing, J. (1988) *Appl. Environ. Microbiol. 54*, 2478−2485.
9. Goyal, A. K., and Zylstra, G. J. (1996) *Appl. Environ. Microbiol. 62*, 230−236.
10. Mobus, E., Jahn, M., Schmid, R., Jahn, D., and Maser, E. (1997) *J. Bacteriol. 179*, 5951−5955.
11. Oppermann, U. C. T., Belai, I., and Maser, E. (1996) *J. Steroid. Biochem. Mol. Biol. 58*, 217−223.
12. Jez, J. M., Flynn, T. G., and Penning, T. M. (1997) *Biochem. Pharmacol. 54*, 639−647.
13. Jörnvall, H., Persson, B., Krook, M., Atrian, S., Gonzàlez-Duarte, R., Jeffery, J., and Ghosh, D. (1995) *Biochemistry 34*, 6003−6013.
14. Oppermann, U. C., Persson, B., Filling, C., and Jornvall, H. (1997) *Adv. Exp. Med. Biol. 414*, 403−415.
15. Yin, S. J., Vagelopoulos, N., Lundquist, G., and Jörnvall, H. (1991) *Eur. J. Biochem. 197*, 359−365.
16. Oppermann, U. C. T., and Maser, E. (1996) *Eur. J. Biochem. 241*, 744−749.
17. Mobus, E., and Maser, E. (1998) *J. Biol. Chem. 273*, 30888−30896.
18. Talalay, P., and Marcus, P. I. (1956) *J. Biol. Chem. 218*, 675−691.
19. Schultz, R. M., Groman, E. V., and Engel, L. L. (1977) *J. Biol. Chem. 252*, 3784−3790.
20. Liras, P., Kasparian, S. S., and Umbreit, W. W. (1975) *Appl. Microbiol. 30*, 650−656.
21. Ringold, H. J., Bellas, T., and Clark, A. (1967) *Biochem. Biophys. Res. Commun. 27*, 361−367.
22. Minard, P., Legoy, M. D., and Thomas, D. (1985) *FEBS Lett. 188*, 85−90.
23. Benach, J., Knapp, S., Oppermann, U. C. T., Hägglund, O., Jörnvall, H., and Ladenstein, R. (1996) *Eur. J. Biochem. 236*, 144−148.
24. Oppermann, U. C. T., Filling, C., Berndt, K. D., Persson, B., Benach, J., Ladenstein, R., and Jörnvall, H. (1997) *Biochemistry 36*, 34−40.
25. Li, B., and Lin, S.-X. (1996) *Eur. J. Biochem. 235*, 180−186.
26. Lu, G. (1999) *J. Appl. Crystallogr. 32*, 375−376.
27. Ghosh, D., Wawrzak, Z., Weeks, C. M., Duax, W. L., and Erman, M. (1994) *Structure 2*, 629−640.
28. Murshudov, G. N., Vagin, A. A., and Dodson, E. J. (1997) *Acta Crystallogr. Sect. D 53*, 240−255.
29. Bricogne, G., and Irvin, J. J. (1996) In *Proceedings of the CCP4 Study Weekend,* pp 85−92, SERC Daresbury Laboratory, Warrington, England.
30. Bricogne, G. (1997) In *Methods in Enzymology* (Carter, C. W. J., and Sweet, R. M., Eds.) pp 361−423, Academic Press.
31. Roversi, P., Blanc, E., Vonrhein, C., Evans, G., and Bricogne, G. (2000) *Acta Crystallogr. Sect. D 56*, 1316−1323.
32. Lamzin, V. S., and Wilson, K. S. (1997) *Methods Enzymol. Biophys. 161*, 227−233.
33. Sheldrick, G. M., and Schneider, T. R. (1997) *Methods Enzymol. 277*, 319−343.
34. Ghosh, D., Erman, M., Wawrzak, Z., Duax, W. L., and Pangborn, W. (1994) *Structure 2*, 973−980.
35. Morris, G. M., Goodsell, D. S., Halliday, R. S., Huey, R., Hart, W. E., Belew, R. K., and Olson, A. J. (1998) *J. Computational Chem. 19*, 1639−1662.
36. Laskowski, R. A., MacArthur, M. W., Moss, D. S., and Thornton, J. M. (1993) *J. Appl. Crystallog. 26*, 283−291.
37. Grimm, C., Maser, E., Mobus, E., Klebe, G., Reuter, K., and Ficner, R. (2000) *J. Biol. Chem. 275*, 41333−41339.
38. Varughese, K. I., Skinner, M. M., Whiteley, J. M., Matthews, D. A., and Xuong, N. H. (1992) *Proc. Natl. Acad. Sci. U.S.A. 89*, 6080−6084.
39. Benach, J., Atrian, S., Gonzàlez-Duarte, R., and Ladenstein, R. (1998) *J. Mol. Biol. 282*, 383−399.
40. Filling, C., Nordling, E., Benach, J., Berndt, K. D., Ladenstein, R., Jörnvall, H., and Oppermann, U. (2001) *Biochem. Biophys. Res. Commun. 289*, 712−717.
41. Filling, C., Berndt, K. D., Benach, J., Knapp, S., Prozorovski, T., Nordling, E., Ladenstein, R., Jörnvall, H., and Oppermann, U. (2002) *J. Biol. Chem. 277*, 25677−25684.
42. Levy, M. A. H., Dennis A.; Brandt, Martin; Metcaf, Brian W. (1987) *Biochemistry 26*, 2270−2279.
43. Keung, W.-M. (1995) *Biochem. Biophys. Res. Comm. 215*, 1137−1144.
44. Tanaka, N., Nonaka, T., Tanabe, T., Yoshimoto, T., Tsuru, D., and Mitsui, Y. (1996) *Biochemistry 35*, 7715−7730.
45. Han, Q., Campbell, R. L., Gangloff, A., Huang, Y. W., and Lin, S. X. (2000) *J. Biol. Chem. 275*, 1105−11.
46. Ghosh, D., Sawicki, M., Pletnev, V., Erman, M., Ohno, S., Nakajin, S., and Duax, W. L. (2001) *J. Biol. Chem. 276*, 18457−63.
47. Nobel, S., Abrahmsen, L., and Oppermann, U. (2001) *Eur. J. Biochem. 268*, 4113−4125.
48. Sawicki, M. W., Erman, M., Puranen, T., Vihko, P., and Ghosh, D. (1999) *Proc. Natl. Acad. Sci. U.S.A. 96*, 840−845.
49. Duax, W. L., Ghosh, D., and Pletnev, V. (2000) *Vitam. Horm. 58*, 121−148.
50. Ghosh, D., and Vihko, P. (2001) *Chem. Biol. Interact. 130−132*, 637−650.
51. Benach, J., Atrian, S., Gonzàlez-Duarte, R., and Ladenstein, R. (1999) *J. Mol. Biol. 289*, 335−355.
52. Carson, M. (1987) *J. Mol. Graphics 5*, 103−106.
53. Kleywegt, G. J., and Jones, T. A. (1994) *Acta Crystallogr. Sect. D 50*, 178−185.

BI0203684